BNL-209816-2018-JAAM

# Phase Diagram of Bi2Sr2CaCu2O8+Delta Revisited

I. K. Drozdov, T. Valla

To be published in "Nature Communications "

December 2018

Condensed Matter Physics and Materials Science Department

**Brookhaven National Laboratory**

**U.S. Department of Energy**

USDOE Office of Science (SC), Basic Energy Sciences (BES) (SC-22)

Notice: This manuscript has been authored by employees of Brookhaven Science Associates, LLC under Contract No. DE-SC0012704 with the U.S. Department of Energy. The publisher by accepting the manuscript for publication acknowledges that the United States Government retains a non-exclusive, paid-up, irrevocable, world-wide license to publish or reproduce the published form of this manuscript, or allow others to do so, for United States Government purposes.

# DISCLAIMER

This report was prepared as an account of work sponsored by an agency of the United States Government. Neither the United States Government nor any agency thereof, nor any of their employees, nor any of their contractors, subcontractors, or their employees, makes any warranty, express or implied, or assumes any legal liability or responsibility for the accuracy, completeness, or any third party's use or the results of such use of any information, apparatus, product, or process disclosed, or represents that its use would not infringe privately owned rights. Reference herein to any specific commercial product, process, or service by trade name, trademark, manufacturer, or otherwise, does not necessarily constitute or imply its endorsement, recommendation, or favoring by the United States Government or any agency thereof or its contractors or subcontractors. The views and opinions of authors expressed herein do not necessarily state or reflect those of the United States Government or any agency thereof.

# Phase Diagram of $Bi_2Sr_2CaCu_2O_{8+\delta}$ Revisited

I. K. Drozdov,[1] I. Pletikosić,[1,2] C.-K. Kim,[1] K. Fujita,[1] G. D. Gu,[1]
J. C. Séamus Davis,[1,3] P. D. Johnson,[1] I. Božović,[1] and T. Valla[1]

[1] *Condensed Matter Physics and Materials Science Department, Brookhaven National Lab, Upton, New York 11973, USA*
[2] *Department of Physics, Princeton University, Princeton, NJ 08544, USA*
[3] *Laboratory of Atomic and Solid State Physics, Department of Physics, Cornell University, Ithaca, NY 14853, USA*

(Dated: November 13, 2018)

In cuprate superconductors, the doping of carriers into the parent Mott insulator induces superconductivity and various other phases whose characteristic temperatures are typically plotted versus the doping level $p$. In most materials, $p$ cannot be determined from the chemical composition, but it is derived from the superconducting transition temperature, $T_c$, using the assumption that $T_c$ dependence on doping is universal. Here, we present angle-resolved photoemission studies of $Bi_2Sr_2CaCu_2O_{8+\delta}$, cleaved and annealed in vacuum or in ozone to reduce or increase the doping from the initial value corresponding to $T_c = 91$ K. We show that $p$ can be determined from the underlying Fermi surfaces and that *in-situ* annealing allows mapping of a wide doping regime, covering the superconducting dome and the non-superconducting phase on the overdoped side. Our results show a surprisingly smooth dependence of the inferred Fermi surface with doping. In the highly overdoped regime, the superconducting gap approaches the value of $2\Delta_0 = (4 \pm 1)k_B T_c$

## INTRODUCTION

$Bi_2Sr_2CaCu_2O_{8+\delta}$ (Bi2212) is a prototypical cuprate High-Tc Superconductor (HTSC) and one of the most studied materials in condensed matter physics. Its phase diagram has been heavily studied by many different techniques. In particular, Bi2212 has been the perfect subject for studies by Angle Resolved Photoemission Spectroscopy (ARPES) and Spectroscopic Imaging - Scanning Tunneling Microscopy (SI-STM) studies due to its ease of cleaving. These techniques have contributed significantly to our current understanding of the cuprates by providing invaluable information on different phenomena and their development with doping, mostly in Bi2212. The $d$-wave symmetry of the superconducting (SC) gap [1, 2], the normal state gap (pseudogap) [3–5], the quasiparticle (QP) self-energy [2, 6, 7] and, more recently, the transition in topology of the Fermi surface (FS) from open to closed [8, 9] are a few notable examples of such contributions. However, Bi2212 can only be doped within a relatively limited range, especially on the overdoped side, where the superconducting transition temperature ($T_c$) cannot be reduced beyond $\sim 50$ K, leaving a large and important region of the phase diagram out of reach. Even within the covered region, the actual doping level $p$ is not independently determined, but it is usually calculated from the measured $T_c$ by assuming the putative parabolic $T_c - p$ dependence that is considered universal for all the cuprates [10]. Only in a very limited number of materials such as $La_{2-x}Sr_xCuO_4$ and $La_{2-x}Ba_xCuO_4$, can the doping be approximately determined from chemical composition as $p \approx x$. These two materials however, have very different $T_c - p$ dependences, illustrating the invalidity of the universal parabolic $T_c - p$ dome [11].

Here, we revisit the Bi2212 phase diagram by modifying the doping level of the as-grown crystal, by annealing *in-situ* cleaved samples either in vacuum, resulting in homogeneous underdoping, or in ozone, resulting in overdoping of the near-surface region. We were able to span a wide region of the phase diagram, ranging from strongly underdoped, with the $T_c$ reduced down to 30 K (UD30), to strongly overdoped, where the superconductivity was completely suppressed (OD0). In addition, we were able to infer the doping level directly from ARPES, by measuring the volume of the underlying Fermi surface. In that way, we follow the development of spectral features with doping with unprecedented clarity and detail and construct the phase diagram of $Bi_2Sr_2CaCu_2O_{8+\delta}$.

## RESULTS

### Fermi Surface

Figure 1 shows the photoemission intensity integrated within $\pm 2.5$ meV around the Fermi level for the as-grown sample and for several different doping levels, induced by annealing in vacuum, or ozone. Due to the presence of the spectral gap, only the near-nodal segments are visible, while the intensity is strongly reduced or absent in most of the Brillouin zone (BZ), except in the highly overdoped samples with reduced gaps. As we move down in energy, more and more of the missing intensity is recovered, and at the energy of the maximal spectral gap ($\Delta_0$), the full, closed contour of the underlying Fermi surface is recovered. Although the Luttinger theorem requires that, to determine the carrier density, one measures the closed contours only for quasiparticles at $E = 0$ (Fermi level), this is rendered impossible by the existence of the spectral gap. Therefore, we hypothesize that the contour

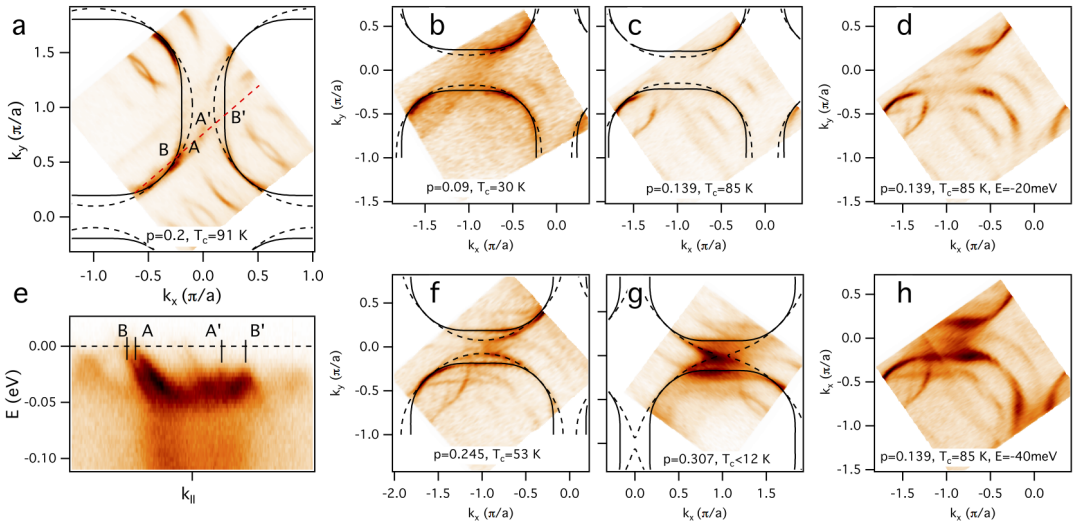


FIG. 1. Development of the electronic structure of $Bi_2Sr_2CaCu_2O_{8+\delta}$ at the Fermi level with doping. (a) Fermi surface of an as grown sample. (b-c) underdoped samples, obtained by annealing of the as grown samples in vacuum. (f-g) overdoped samples, obtained by annealing of as grown samples in $O_3$. Spectral intensity, represented by the false color contours, is integrated within $\pm 2.5$ meV around the Fermi level. Solid (dashed) lines represent the bonding (antibonding) states obtained from the tight-binding approximation that best fits the experimental data. The fitting involved the lines connecting the experimental minimal gap loci in all cases where the underlaying Fermi surface was gapped, as indicated in (e). (e) Dispersion of states along the red dashed line in (a). Fermi momenta of bonding (B, B') and antibonding (A, A') are marked in both (a) and (e). Gapped Fermi momenta (A', B') were approximated by the points where the dispersion acquire maximum. (d) Intensity contour for sample UD85 (from panel (c)) at $E = -20$ meV and (h) $E = -40$ meV. The area enclosed by the TB lines that best represent the experimental data is calculated and used for determination of the doping parameter $p_A$. The superconducting transition temperature, $T_c$, is determined from magnetic susceptibility measurements (as grown and underdoped samples) and from ARPES data, as explained in the text. All the maps were recorded at 12-20 K.

of minimum gap energy may be used for the same purpose. This hypothesis assumes particle-hole symmetry of the gapped state about the chemical potential. In that case, connecting the $(k_x, k_y)$ points where the intensity first appears, yields the curves of minimal gap loci, which we refer to throughout as the underlying Fermi surfaces. Mapping at higher temperatures, above $T_c$ and above the pseudogap temperature, $T^*$, that was performed at several doping levels (see Methods section), shows exactly the same Fermi contours, supporting our approach. We do not see any change in shape between the low- and high-temperature Fermi contours that were previously reported in ref. [12]. Figure 1 also shows tight binding (TB) contours, with solid (dashed) lines representing the bonding (antibonding) states [13–15]. The TB parameters for several doping levels are given in the Methods section. The number of carriers forming the underlying Fermi surface is obtained from the Luttinger count of the area enclosed by the Fermi contour, $p_L = 2A_{FS}$. To express this in terms of doping that usually serves as the abscissa in phase diagrams of the cuprates, we calculate the number of additional holes doped into the parent Mott insulator as $p_A = p_L - 1 = 2A_{FS} - 1$. Here, both the bonding and the antibonding states are counted, $A_{FS} = (A_B + A_A)/2$, originating from two Cu-O planes per unit cell, and the area of the BZ is set to one. We now have an independent doping parameter for $Bi_2Sr_2CaCu_2O_{8+\delta}$ and do not have to rely on the universal dome when plotting the phase diagram.

We note that $p_A$ differs from the concentration of mobile carriers contributing to transport, $p_{tr}$, a quantity that has been difficult to measure directly and accurately. However, recent models and high field studies have indicated that the mobile hole density switches from $p_{tr} \sim p_A$ in the underdoped samples to $p_{tr} \sim p_L = p_A + 1$ near optimal doping [16–18].

In this study, the underlying Fermi surface shows a smooth development with doping, with no evidence for the transition from a small Fermi pocket to big Fermi surface. Due to the structural supermodulation, multiple diffracted replicas of the intrinsic band structure are observed in addition to the shadow Fermi surface, shifted by $(\pi/a, \pi/a)$ [13, 14]. The intrinsic underlying Fermi surface keeps the same topology across most of the doping regime: the two big Fermi surfaces, corresponding to the bonding and antibonding states, resolved in all but the least doped (UD30) sample, remain hole-like. Only at the highest doping levels, where the superconductiv-

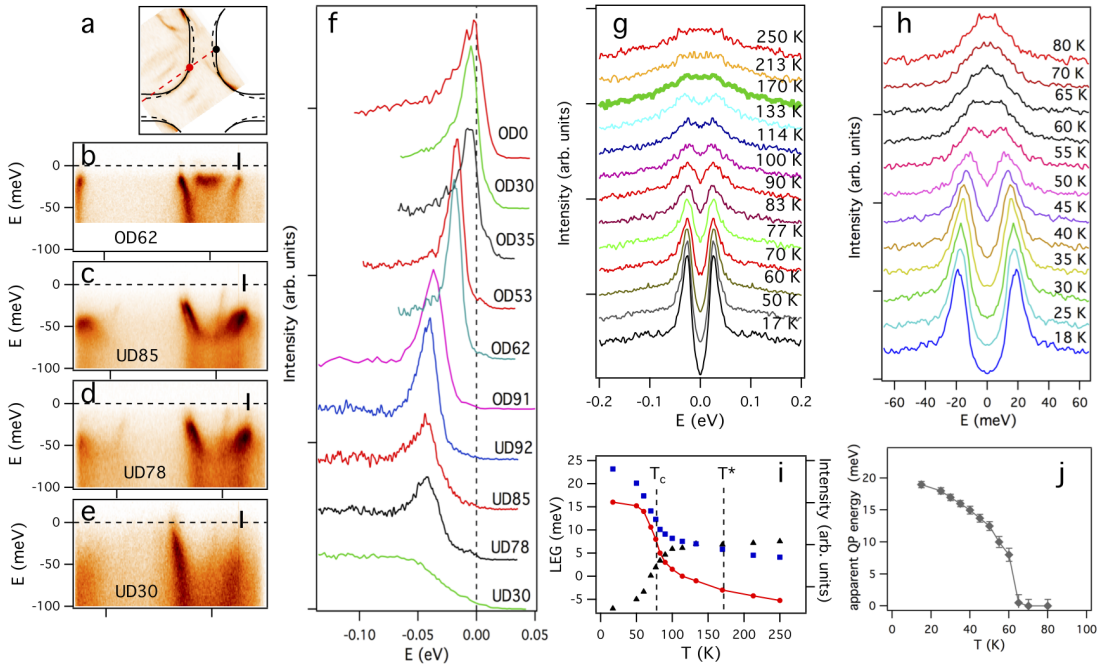


FIG. 2. Spectral gap from the anti-nodal region of $Bi_2Sr_2CaCu_2O_{8+\delta}$. (a) Fermi surface of the UD85 sample, with the dashed red line indicating the momentum line that is probed in the panels (b-e) for samples with different oxygen content. (b-e) ARPES intensity as a function of binding energy and momentum along the dashed line in (a), taken at $T = 12$ K, for several different doping levels, as indicated. (f) The EDC curves taken at the Fermi wave-vector of the bonding state from the anti-nodal region of the Fermi surface, as indicated by bars in panels (b-e). (g) Temperature dependence of ARPES spectra for the underdoped sample, UD78, ($T_c = 78$ K) and (h) for the overdoped sample, OD62 ($T_c = 62$ K). The spectra in (g) and (h) are taken at $k_F$ marked with red and black dots in (a), respectively. Spectra in (g) and (h) are symmetrized relative to the Fermi level. (i-j) Temperature dependence of several spectral parameters for the two samples shown in (g) and (h): intensity at the Fermi level (black triangles) and at the peak energy (blue squares), Leading edge gap (LEG) of non-symmetrized spectra (red circles) and apparent quasiparticle peak position (gray diamonds). The error bars in (j) correspond to the fitting uncertainties in the apparent quasiparticle peak positions from (h).

ity gets suppressed beyond our limits of detection, the antibonding Fermi surface undergoes the Lifshitz transition and becomes an electron pocket centered at $(0, 0)$. No conventional reconstruction of the underlying Fermi surface is visible in our data that we can assign to the charge or spin orders observed in some other cuprates [18–21]. On the contrary, the observed smooth development with doping would imply that the underlying electronic structure of Bi2212 could be approximated by the same TB bands filled to different levels (Table 1 in the Methods section), in line with the recent proposal by Pelc *et al* [22]. Also, the effects of charge ordering observed in the single-layer compound $(Bi,Pb)_2(Sr,La)_2CuO_{6+\delta}$ by Comin *et al* [23], but not by Kondo *et al* [24], do not show up in any of our samples. We also do not observe changes in $k$-space coherence of the low-energy quasiparticle excitations when they cross the antiferromagnetic zone boundary [9]. In all samples studied here in the superconducting phase, quasiparticles retain coherence on both sides of this boundary.

Our study, however, does confirm that the actual Fermi surface of Bi2212 is strongly affected by the pseudogap, i.e. it is partially gapped in the normal state in the wide portion of the phase diagram [2–4, 8]. Our findings are consistent with the general notion that the electronic states cross the Fermi level only in the nodal region, forming the so-called Fermi arcs that grow in length with increasing doping and eventually enclose the whole underlying FS. Whether these arcs arise due to the gap closing, or its filling is still debated [25–27], but the general picture is in line with modern $k$-resolved calculations based on Mott physics that reproduce the nodal-antinodal dichotomy observed in experiments [28]. We note that the Fermi arcs cannot be distinguished from the small Fermi pockets in which only one side is observable, while the other is invisible due to the zero spectral weight [8, 9, 29]. For similar reasons, the observed maps cannot exclude the existence of a pair density wave state, as the relevant portions of reconstructed Fermi surface also carry a vanishing spectral weight in that scenario [30]. To differentiate between these pictures, further theoretical and experimental studies will be required.

### Spectral Gap

In the following, we extract the spectral gap and $T_c$ of each modified sample in order to reconstruct the appropriate phase diagram for $Bi_2Sr_2CaCu_2O_{8+\delta}$. Vacuum annealing results in a seemingly homogeneous doping profile with the surface $T_c$ measured by ARPES showing good agreement with the bulk susceptibility measurements. Thus, on the underdoped side, we usually have two independent measurements of $T_c$. However, annealing in ozone results in increased doping only in the near-surface region. Therefore, the only measure of $T_c$ in the overdoped regime was spectroscopic: the temperature induced changes in the quasiparticle peak intensity, as well as the leading edge position clearly indicate $T_c$ [2, 27].

Figure 2 shows the total spectral gap from the antinodal region ($\Delta_0$) and its temperature dependence for several selected samples with different doping levels. At the antinodal point the $d$-wave superconducting gap has its maximal amplitude. The normal state gap (pseudogap) is also maximal there [2–4, 8, 31]. The energy distribution curves from that point, shown in Fig.2(f), clearly indicate that the quasiparticle peak is shifting closer to the Fermi level as the doping increases, reflecting the reduction of the spectral gap. Also shown is the typical temperature dependence of the spectra for an underdoped sample (UD78) and an overdoped sample (OD62). For the underdoped sample, the gap does not close at $T_c$ determined from susceptibility measurements, but at some higher temperature $T^*$. However, the leading edge gap and intensity of the QP peak show a prominent change around $T_c$ and the later could be identified as being near the inflection point of these temperature dependencies (Fig. 2(i-j)) [27].

### Phase Diagram

The antinodal gap magnitude, $\Delta_0$ is determined from the symmetrized spectra as the position of the quasiparticle peak and plotted in Fig.3 for all the doping levels covered in this study. The superconducting transition temperature, $T_c$, is also plotted. We first note that most of our data agree well with previous studies; gaps and transition temperatures from the present study follow the same trends with very little discrepancies [2, 5, 32–37]. The only adjustment needed for the perfect overlap with the previous studies was the shift in the doping level $p_A$. The superconducting dome for $Bi_2Sr_2CaCu_2O_{8+\delta}$ is now centered at $p_A = 0.18$. Its width remained approximately the same, in agreement with another study that reported the shift [38]. The data from the literature are placed in accordance to the new doping scale.

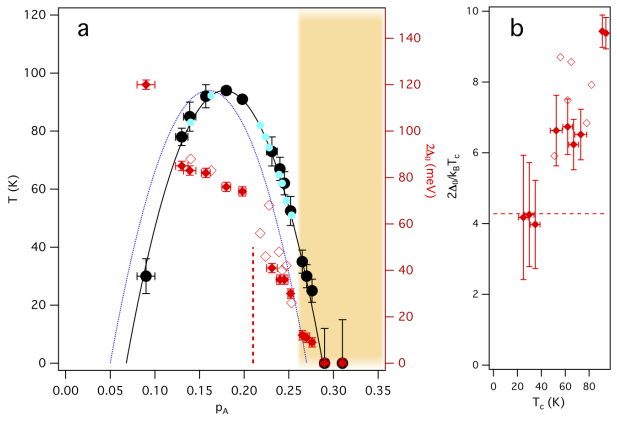


FIG. 3. Phase diagram of $Bi_2Sr_2CaCu_2O_{8+\delta}$. (a) Experimentally obtained superconducting transition temperature, $T_c$, (black circles) and the antinodal gap, $2\Delta_0$ (solid red diamonds) are plotted versus experimentally determined doping parameter, $p_A$. Also shown are gap values (open red diamonds) and $T_c$ (turquoise circles) for different doping levels from several previously published studies [5, 32–34]. These points are placed at the corresponding $p_A$ in accordance with our new $T_c(p_A)$ dependence. The universal superconducting dome is shown as blue dashed line, while the corrected dome is represented by black solid line. The red dashed line indicates the transition observed in SI-STM studies [9]. The shaded area marks the region that has not been studied before. Characteristic temperatures are displayed against the left axis, while the right axis is for the spectral gap. (b) Ratio of the antinodal gap and $T_c$ for the points shown in (a) from the overdoped side. The red dashed line corresponds to the BCS value for $d$-wave gap. We have approximated the uncertainty in doping, $\Delta p_A$, (horizontal error bars in (a)) to be proportional to the width of the Fermi surface: $\Delta p_A/p_A \sim 2\Delta k_F/k_F$. The uncertainty in $T_c$ is given by the width of superconducting transition in susceptibility measurements (underdoped samples), or by the temperature step size in $T$-dependent ARPES measurements that identify $T_c$ (overdoped samples). The uncertainty in gap magnitude (red vertical error bars in (a)) corresponds to the standard deviation of the quasiparticle peak position determined from fitting. It serves to determine the propagated uncertainty (vertical error bars) in (b).

## DISCUSSION

The important new ingredient of the re-drawn phase diagram (Fig.3) is the completely new doping regime that is covered by this study (represented with the shaded area in Fig.3(a)): the highly overdoped regime, far beyond what was previously explored in Bi2212, has now been mapped, including the critical point at which superconductivity vanishes. As shown in Fig.3(b), it is only in this regime ($p_A > 0.25$) that $2\Delta_0/(k_BT_c)$ actually acquires low values consistent with those inferred by extrapolation from less overdoped regime in previous studies [39].

With further increase in doping, both the gap and $T_c$

vanish around $p_A = 0.29$ and Bi2212 is no longer a superconductor. It is intriguing that this coincides with the change in Fermi surface topology: the antibonding Fermi surface undergoes a conventional Lifshitz transition, turning from a hole-like into an electron-like, as its saddle points at $(\pm\pi/a, 0$ and $(0, \pm\pi/a)$ move above the Fermi level. The coincidence of these two transitions hints at the importance of the Fermi surface topology for superconductivity in the cuprates, but its exact role remains unclear. In the single layer counterpart, $(Bi,Pb)_2(Sr,La)_2CuO_{6+\delta}$, the Lifshitz transition is also coincidental with vanishing superconductivity [24]. This material, moreover, shows much more drastic departure from the universal superconducting dome, with the maximal $T_c$ occurring near $p_A = 0.3$. In $Bi_2Sr_2CaCu_2O_{8+\delta}$, the Lifshitz transition affects only one FS and not the other. This would suggest that the changes in the antibonding state are for some reason more important for superconductivity than those in the bonding state. At this moment, it is not clear why this should be the case. One suggestion could be that the straight segments of the bonding state's Fermi surface are susceptible to nesting and are involved in charge, spin or pair density waves, instead of superconductivity. However, in this highly overdoped regime, the lack of a gap and other effects that these phenomena should induce into the spectral response certainly argues against this scenario. Still, it seems that the curvature (or a lack of it) of the Fermi surface in the antinodal region plays a significant role in cuprate superconductivity and that the straight antinodal segments of the FS might be ineffective in forming the efficient singlet pairs even when not contributing to density waves. This might be because the group velocity of these straight segments lacks the component that would connect them from $\mathbf{k_F}$ to $-\mathbf{k_F}$ into singlet pairs. Further studies on other multi-layered cuprate superconductors will be necessary to resolve these questions.

## METHODS

### Sample Preparation

The experiments within this study were done in a new experimental facility that integrates oxide-MBE with ARPES and STM capabilities within the common vacuum system [40]. The starting samples were slightly overdoped ($T_c = 91$ K) single-crystals of $Bi_2Sr_2CaCu_2O_{8+\delta}$, synthesized by the traveling floating zone method. They were clamped to the sample holder and cleaved with Kapton tape in the ARPES preparation chamber (base pressure of $3 \times 10^{-8}$ Pa). Thus, the silver-epoxy glue, commonly used for mounting samples and associated processing at elevated temperatures, has been completely eliminated, resulting in perfectly flat cleaved surfaces and unaltered doping level.

The cleaved samples were then annealed *in-situ* in the ARPES preparation chamber to different temperatures ranging from 150 to 700°C for several hours, resulting in the loss of oxygen and underdoping. For the overdoping, the cleaved as-grown samples were transfered to the MBE chamber (base pressure of $8 \times 10^{-8}$ Pa) where they were annealed in $3 \times 10^{-3}$ Pa of cryogenically distilled $O_3$ at 350-480°C for $\approx 1$ hour. After the annealing, films were cooled to room temperature in the ozone atmosphere and transfered to the ARPES chamber (base pressure of $8 \times 10^{-9}$ Pa. Vacuum annealing results in generally homogeneous doping profile where the surface $T_c$ measured by ARPES shows no variation with repeated re-cleaving of the annealed crystals and is in a good agreement with the bulk susceptibility measurements. Annealing of as grown crystals in $O_3$ results in increased doping in the near-surface region, as evidenced by the increased hole Fermi surface, reduced spectral gap and its closing temperature. The most of the crystal's volume remained near the optimal doping upon ozone annealing. The thickness of the overdoped surface layer was in the sub-micron range, as only the thinnest, semi-transparent re-cleaved flakes showed the significant reduction in $T_c$ in susceptibility measurements.

### ARPES

The ARPES experiments were carried out on a Scienta SES-R4000 electron spectrometer with the monochromatized HeI (21.22 eV) radiation (VUV-5k). The total instrumental energy resolution was $\sim 5$ meV. Angular resolution was better than $\sim 0.15°$ and $0.4°$ along and perpendicular to the slit of the analyzer, respectively.

The ARPES estimate of $T_c$ of the overdoped surfaces was within $\pm 4$ K, except for the two samples falling outside of the superconducting dome, for which the estimate was limited by the base temperature that could be reached with our cryostat (12 and 15 K, for these two cases).

Maps of the underlying Fermi surfaces in the superconducting state (gapped state) agree perfectly well with fully enclosed Fermi surface contours obtained in the state without any spectral gaps at $T > T^* > T_c$ as was checked for several samples, including the OD91, UD87 (Fig.4) and several overdoped samples. Positions of minimal gap loci in the SC state overlap with the positions of Fermi momenta in the normal (gapless) state within the experimental resolution.

### Tight Binding Parameters

The bare in-plane band structure of $Bi_2Sr_2CaCu_2O_{8+\delta}$ used to fit the experimental FS contours is approximated

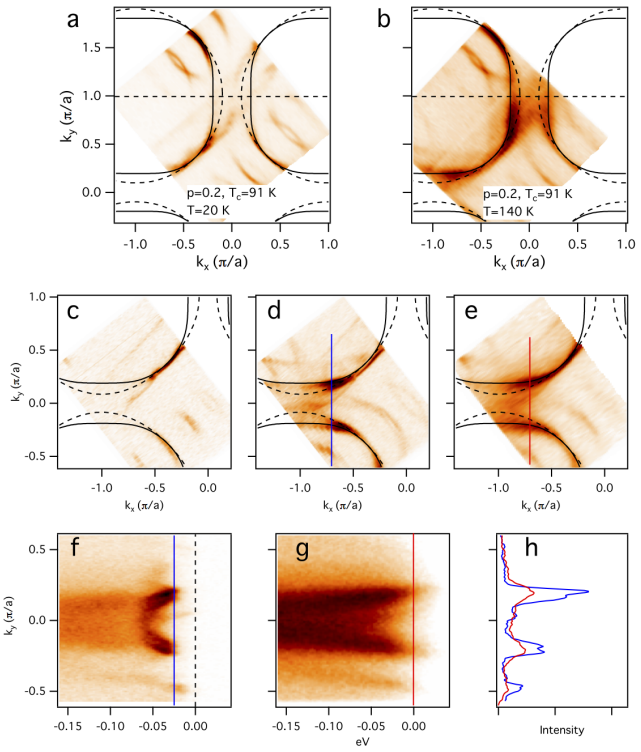


FIG. 4. Comparison of the underlying gapped FS with the gapless FS. (a) FS contour in the superconducting state and (b) fully enclosed FS contour obtained in the normal state, at $T = 140$ K ($> T^*$) for the as grown sample, OD91. The TB parameters are identical in both panels. (c) Constant energy contour at $E = 0$ and (d) at $E = -25$ meV in the superconducting state ($T = 20$ K) of the underdoped sample, UD87. (e) The normal state contour at $E = 0$ of the same sample ($T = 125$ K). The TB contours are identical in (c, d and e). (f) and (g) show the photoemission intensities along the momentum lines indicated in (d) and (e), $k_x = -0.7\ \pi a^{-1}$ in the superconducting and normal states, respectively. (h) Momentum distribution curves at $E = -25$ meV and at $E = 0$, with the maxima corresponding to the gapped and gapless Fermi momenta from (f) and (g), respectively.

by the tight-binding formula:

$$E_{\mathrm{A,B}}(k) = \mu - 2t(\cos k_x + \cos k_y) + 4t' \cos k_x \cos k_y - 2t''(\cos 2k_x + \cos 2k_y) \pm t_\perp (\cos k_x - \cos k_y)^2/4, \quad (1)$$

where the index A (B) is for anti-bonding (bonding) state and $\mu$ is chemical potential. The hopping parameters that best describe the Fermi surfaces of selected measured samples are given in Table I.

The TB contours that agree with the experimental contours the best were chosen by eye. By changing them to the point where discrepancies would become clearly visible, we can estimate that the uncertainty in doping, $\Delta p_{\mathrm{A}}$, of this method is very close to that estimated from the experimental momentum width of the Fermi surface, $\Delta p_{\mathrm{A}}/p_{\mathrm{A}} \sim 2\Delta k_{\mathrm{F}}/k_{\mathrm{F}}$ .

TABLE I. Tight binding parameters for $Bi_2Sr_2CaCu_2O_{8+\delta}$

| Sample | $\mu$ (meV) | $t$ (meV) | $t'$ (meV) | $t''$ (meV) | $t_\perp$ (meV) |
|---|---|---|---|---|---|
| UD30 | 340 | 390 | 120 | 45 | 108 |
| UD78 | 330 | 350 | 100 | 45 | 95 |
| OD91 | 405 | 360 | 108 | 36 | 108 |
| OD67 | 430 | 360 | 108 | 36 | 108 |
| OD35 | 445 | 360 | 108 | 36 | 108 |
| OD0 | 467 | 360 | 108 | 36 | 108 |

The electronic structure of Bi2212 could be approximated by nearly the same TB parameters in the whole doping range covered in this study, indicating that our data show no evidence for dramatic transitions involving charge/spin ordered states with substantial spectral weight redistribution as doping is swept from strongly underdoped ($p = 0.09$) to strongly overdoped, non-superconducting ($p > 0.29$) regime. This observation suggests that in the studied doping range, the underlying electronic structure of Bi2212 can, in essence, be described as the progressive filling of the same bilayer split bands, with spectral gaps and pseudogaps as additional necessary ingredients in superconducting samples.

## DATA AVAILABILITY

The data that support the findings of this study are available from the corresponding author upon reasonable request. The source data underlying Figs 2j and 3a-b are provided as a Source Data file.


[1] Z.-X. Shen, D. S. Dessau, B. O. Wells, D. M. King, W. E. Spicer, A. J. Arko, D. Marshall, L. W. Lombardo, A. Kapitulnik, P. Dickinson, S. Doniach, J. DiCarlo, T. Loeser, and C. H. Park. *Anomalously large gap anisotropy in the a - b plane of $Bi_2Sr_2CaCu_2O_{8+\delta}$.* Physical Review Letters, **70**, 1553–1556 (1993).

[2] A. Damascelli, Z. Hussain, and Z.-X. Shen. *Angle-resolved photoemission studies of the cuprate superconductors.* Reviews of Modern Physics, **75**, 473 (2003).

[3] H. Ding, T. Yokoya, J. C. Campuzano, T. Takahashi, M. Randeria, M. R. Norman, T. Mochiku, K. Kadowaki, and J. Giapintzakis. *Spectroscopic evidence for a pseudogap in the normal state of underdoped high-T c superconductors.* Nature, **382**, 51–54 (1996).

[4] D. S. Marshall, D. S. Dessau, A. G. Loeser, C.-H. Park, A. Y. Matsuura, J. N. Eckstein, I. Bozovic, P. Fournier, A. Kapitulnik, W. E. Spicer, and Z.-X. Shen. *Unconventional Electronic Structure Evolution with Hole Doping in $Bi_2Sr_2CaCu_2O_{8+\delta}$ : Angle-Resolved Photoemission Results.* Physical Review Letters, **76**, 4841–4844 (1996).

[5] C. Renner, B. Revaz, J.-Y. Genoud, K. Kadowaki, and Ø. Fischer. *Pseudogap Precursor of the Superconducting Gap in Under- and Overdoped $Bi_2Sr_2CaCu_2O_{8+\delta}$*. Physical Review Letters, **80**, 149–152 (1998).

[6] T. Valla, A. V. Fedorov, P. D. Johnson, B. O. Wells, S. L. Hulbert, Q. Li, G. D. Gu, and N. Koshizuka. *Evidence for Quantum Critical Behavior in the Optimally Doped Cuprate $Bi_2Sr_2CaCu_2O_{8+\delta}$*. Science, **285**, 2110–2113 (1999).

[7] P. Johnson, T. Valla, A. Fedorov, Z. Yusof, B. Wells, Q. Li, A. Moodenbaugh, G. Gu, N. Koshizuka, C. Kendziora, S. Jian, and D. Hinks. *Doping and Temperature Dependence of the Mass Enhancement Observed in the Cuprate $Bi_2Sr_2CaCu_2O_{8+\delta}$*. Physical Review Letters, **87**, 177007 (2001).

[8] H.-B. Yang, J. D. Rameau, Z.-H. Pan, G. D. Gu, P. D. Johnson, H. Claus, D. G. Hinks, and T. E. Kidd. *Reconstructed Fermi Surface of Underdoped $Bi_2Sr_2CaCu_2O_{8+\delta}$ Cuprate Superconductors*. Physical Review Letters, **107**, 047003 (2011).

[9] K. Fujita, C. K. Kim, I. Lee, J. Lee, M. H. Hamidian, I. A. Firmo, S. Mukhopadhyay, H. Eisaki, S. Uchida, M. J. Lawler, E.-A. Kim, J. C. Davis, H. Ikuta, P. Mistark, R. S. Markiewicz, A. Bansil, S. Sachdev, E. W. Hudson, and J. E. Hoffman. *Simultaneous transitions in cuprate momentum-space topology and electronic symmetry breaking*. Science (New York, N.Y.), **344**, 612–6 (2014).

[10] S. D. Obertelli, J. R. Cooper, and J. L. Tallon. *Systematics in the thermoelectric power of high- Tc oxides*. Physical Review B, **46**, 14928–14931 (1992).

[11] A. R. Moodenbaugh, Y. Xu, M. Suenaga, T. J. Folkerts, and R. N. Shelton. *Superconducting properties of $La_{2-x}Ba_xCuO_4$*. Physica C Superconductivity, **38**, 4596 (1988).

[12] R.-H. He, M. Hashimoto, H. Karapetyan, J. D. Koralek, J. P. Hinton, J. P. Testaud, V. Nathan, Y. Yoshida, H. Yao, K. Tanaka, W. Meevasana, R. G. Moore, D. H. Lu, S.-K. Mo, M. Ishikado, H. Eisaki, Z. Hussain, T. P. Devereaux, S. A. Kivelson, J. Orenstein, A. Kapitulnik, and Z.-X. Shen. *From a Single-Band Metal to a High-Temperature Superconductor via Two Thermal Phase Transitions*. Science, **331**, 1579–1583 (2011).

[13] M. R. Norman, M. Randeria, H. Ding, and J. C. Campuzano. *Phenomenological models for the gap anisotropy of $Bi_2Sr_2CaCu_2O_{8+\delta}$ as measured by angle-resolved photoemission spectroscopy*. Physical Review B, **52**, 615–622 (1995).

[14] H. Ding, A. F. Bellman, J. C. Campuzano, M. Randeria, M. R. Norman, T. Yokoya, T. Takahashi, H. Katayama-Yoshida, T. Mochiku, K. Kadowaki, G. Jennings, and G. P. Brivio. *Electronic Excitations in $Bi_2Sr_2CaCu_2O_{8+\delta}$ : Fermi Surface, Dispersion, and Absence of Bilayer Splitting*. Physical Review Letters, **76**, 1533–1536 (1996).

[15] R. S. Markiewicz, S. Sahrakorpi, M. Lindroos, H. Lin, and A. Bansil. *One-band tight-binding model parametrization of the high- Tc cuprates including the effect of $k_z$ dispersion*. Physical Review B, **72**, 054519 (2005).

[16] Y. Ando, Y. Kurita, S. Komiya, S. Ono, and K. Segawa. *Evolution of the Hall Coefficient and the Peculiar Electronic Structure of the Cuprate Superconductors*. Physical Review Letters, **92**, 197001 (2004).

[17] L. P. Gor'kov and G. B. Teitel'baum. *Interplay of Externally Doped and Thermally Activated Holes in $La_{2-x}Sr_xCuO_4$ and Their Impact on the Pseudogap Crossover*. Physical Review Letters, **97**, 247003 (2006).

[18] S. Badoux, W. Tabis, F. Laliberté, G. Grissonnanche, B. Vignolle, D. Vignolles, J. Béard, D. A. Bonn, W. N. Hardy, R. Liang, N. Doiron-Leyraud, L. Taillefer, and C. Proust. *Change of carrier density at the pseudogap critical point of a cuprate superconductor*. Nature, **531**, 210–214 (2016).

[19] N. Doiron-Leyraud, C. Proust, D. LeBoeuf, J. Levallois, J.-B. Bonnemaison, R. Liang, D. A. Bonn, W. N. Hardy, and L. Taillefer. *Quantum oscillations and the Fermi surface in an underdoped high-Tc superconductor*. Nature, **447**, 565–568 (2007).

[20] G. Ghiringhelli, M. Le Tacon, M. Minola, S. Blanco-Canosa, C. Mazzoli, N. B. Brookes, G. M. De Luca, A. Frano, D. G. Hawthorn, F. He, T. Loew, M. Moretti Sala, D. C. Peets, M. Salluzzo, E. Schierle, R. Sutarto, G. A. Sawatzky, E. Weschke, B. Keimer, and L. Braicovich. *Long-range incommensurate charge fluctuations in (Y,Nd)$Ba_2Cu_3O_{6+x}$*. Science (New York, N.Y.), **337**, 821–5 (2012).

[21] T. Wu, H. Mayaffre, S. Krämer, M. Horvatić, C. Berthier, W. N. Hardy, R. Liang, D. A. Bonn, and M.-H. Julien. *Magnetic-field-induced charge-stripe order in the high-temperature superconductor $YBa_2Cu_3O_y$*. Nature, **477**, 191–194 (2011).

[22] D. Pelc, P. Popčević, G. Yu, M. Požek, M. Greven, and N. Barišić. *Unusual behavior of cuprates explained by heterogeneous charge localization*. https://arxiv.org/abs/1710.10221 (2017).

[23] R. Comin, A. Frano, M. M. Yee, Y. Yoshida, H. Eisaki, E. Schierle, E. Weschke, R. Sutarto, F. He, A. Soumyanarayanan, Y. He, M. Le Tacon, I. S. Elfimov, J. E. Hoffman, G. A. Sawatzky, B. Keimer, and A. Damascelli. *Charge order driven by Fermi-arc instability in $Bi_2Sr_{2-x}La_xCuO_{6+\delta}$*. Science (New York, N.Y.), **343**, 390–2 (2014).

[24] T. Kondo, T. Takeuchi, T. Yokoya, S. Tsuda, S. Shin, and U. Mizutani. *Hole-concentration dependence of band structure in (Bi,Pb)$_2$(Sr,La)$_2CuO_{6+\delta}$ determined by the angle-resolved photoemission spectroscopy*. Journal of Electron Spectroscopy and Related Phenomena, **137-140**, 663–668 (2004).

[25] A. Kanigel, M. R. Norman, M. Randeria, U. Chatterjee, S. Souma, A. Kaminski, H. M. Fretwell, S. Rosenkranz, M. Shi, T. Sato, T. Takahashi, Z. Z. Li, H. Raffy, K. Kadowaki, D. Hinks, L. Ozyuzer, and J. C. Campuzano. *Evolution of the pseudogap from Fermi arcs to the nodal liquid*. Nature Physics, **2**, 447–451 (2006).

[26] T. J. Reber, N. C. Plumb, Z. Sun, Y. Cao, Q. Wang, K. McElroy, H. Iwasawa, M. Arita, J. S. Wen, Z. J. Xu, G. Gu, Y. Yoshida, H. Eisaki, Y. Aiura, and D. S. Dessau. *The origin and non-quasiparticle nature of Fermi arcs in $Bi_2Sr_2CaCu_2O_{8+\delta}$*. Nature Physics, **8**, 606–610 (2012).

[27] T. Kondo, W. Malaeb, Y. Ishida, T. Sasagawa, H. Sakamoto, T. Takeuchi, T. Tohyama, and S. Shin. *Point nodes persisting far beyond Tc in Bi2212*. Nature Communications, **6**, 7699 (2015).

[28] M. Ferrero, P. S. Cornaglia, L. De Leo, O. Parcollet, G. Kotliar, and A. Georges. *Pseudogap opening and formation of Fermi arcs as an orbital-selective Mott transition in momentum space*. Physical Review B, **80**, 064501

(2009).
[29] K.-Y. Yang, T. M. Rice, and F.-C. Zhang. *Phenomenological theory of the pseudogap state.* Physical Review B, **73**, 174501 (2006).
[30] M. R. Norman and J. C. S. Davis. *Quantum oscillations in a biaxial pair density wave state.* Proceedings of the National Academy of Sciences of the United States of America, **115**, 5389–5391 (2018).
[31] T. Valla, A. V. Fedorov, J. Lee, J. C. Davis, and G. D. Gu. *The ground state of the pseudogap in cuprate superconductors.* Science (New York, N.Y.), **314**, 1914–6 (2006).
[32] L. Ozyuzer, J. F. Zasadzinski, C. Kendziora, and K. E. Gray. *Quasiparticle and Josephson tunneling of overdoped $Bi_2Sr_2CaCu_2O_{8+\delta}$ single crystals.* Physical Review B, **61**, 3629–3640 (2000).
[33] Z. Yusof, B. Wells, T. Valla, A. Fedorov, P. Johnson, Q. Li, C. Kendziora, S. Jian, and D. Hinks. *Quasiparticle Liquid in the Highly Overdoped $Bi_2Sr_2CaCu_2O_{8+\delta}$.* Physical Review Letters, **88**, 167006 (2002).
[34] K. K. Gomes, A. N. Pasupathy, A. Pushp, S. Ono, Y. Ando, and A. Yazdani. *Visualizing pair formation on the atomic scale in the high-Tc superconductor $Bi_2Sr_2CaCu_2O_{8+\delta}$.* Nature, **447**, 569–572 (2007).
[35] J. Hwang, T. Timusk, and G. D. Gu. *High-transition-temperature superconductivity in the absence of the magnetic-resonance mode.* Nature, **427**, 714–717 (2004).
[36] B. Keimer, S. A. Kivelson, M. R. Norman, S. Uchida, and J. Zaanen. *From quantum matter to high-temperature superconductivity in copper oxides.* Nature, **518**, 179–186 (2015).
[37] S. Benhabib, A. Sacuto, M. Civelli, I. Paul, M. Cazayous, Y. Gallais, M.-A. Méasson, R. D. Zhong, J. Schneeloch, G. D. Gu, D. Colson, and A. Forget. *Collapse of the Normal-State Pseudogap at a Lifshitz Transition in the $Bi_2Sr_2CaCu_2O_{8+\delta}$ Cuprate Superconductor.* Physical Review Letters, **114**, 147001 (2015).
[38] Y. Zhang, C. Hu, Y. Hu, L. Zhao, Y. Ding, X. Sun, A. Liang, Y. Zhang, S. He, D. Liu, L. Yu, G. Liu, X. Dong, G. Gu, C. Chen, Z. Xu, and X. Zhou. *In situ carrier tuning in high temperature superconductor $Bi_2Sr_2CaCu_2O_{8+\delta}$ by potassium deposition.* Science Bulletin, **61**, 1037–1043 (2016).
[39] A. Ino, H. Anzai, M. Arita, H. Namatame, M. Taniguchi, M. Ishikado, K. Fujita, S. Ishida, and S. Uchida. *Doping dependence of low-energy quasiparticle excitations in superconducting Bi2212.* Nanoscale Research Letters, **8**, 515 (2013).
[40] C. K. Kim, I. K. Drozdov, K. Fujita, J. C. S. Davis, I. Božović, and T. Valla. *In-situ angle-resolved photoemission spectroscopy of copper-oxide thin films synthesized by molecular beam epitaxy.* in press, https://doi.org/10.1016/j.elspec.2018.07.003 (2018).

## ACKNOWLEDGEMENTS

We thank J. Tranquada, R. Konik and J. Misewich for discussions. This work was supported by the US Department of Energy, Office of Basic Energy Sciences, contract no. DE-AC02-98CH10886. I.P. is supported by ARO MURI program, grant W911NF-12-1-0461. I.K.D. acknowledges the generous financial support of the BNL Gertrude and Maurice Goldhaber Distinguished Fellowship.

## AUTHOR INFORMATION

### Affiliations

Condensed Matter Physics and Materials Science Department, Brookhaven National Lab, Upton, New York 11973, USA
I. K. Drozdov, I. Pletikosić, C.-K. Kim, K. Fujita, G. D. Gu, J. C. Séamus Davis, P. D. Johnson, I. Božović and T. Valla
Department of Physics, Princeton University, Princeton, NJ 08544, USA
I. Pletikosić
Laboratory of Atomic and Solid State Physics, Department of Physics, Cornell University, Ithaca, NY 14853, USA
J. C. Séamus Davis

### Contributions

I.K.D. and T.V. designed and directed the study. G.D.G. grew the bulk crystals and performed magnetization measurements. I.K.D. performed the sample preparation in ozone. I.P. and T.V. performed the ARPES experiments. T.V. analyzed and interpreted data and wrote the manuscript. I.K.D., I.P., C.K.K., K.F., J.C.S.D., P.D.J., I.B and T.V. made contributions to development of the OASIS facility used herein and commented on the manuscript.

### Competing interests

The authors declare no competing interests.

### Corresponding author

Correspondence should be addressed to T.V. (valla@bnl.gov).